Free streamline and jet flows by vortex boundary integral modeling

R. I. Lewis
Department of Mechanical, Materials and Manufacturing Engineering,
University of Newcastle upon Tyne, UK

The surface vorticity boundary integral method for incompressible, inviscid, irrotational flow is extended to deal with flow problems that include free shear layers. A numerical framework is presented to estimate free streamline and jet flows. The analysis is also applied to the simulation of an airfoil situated in an open jet wind tunnel.

Keywords: boundary integral; vortex sheet; free streamlines; jets

1.0 Introduction

Prior to 1980, boundary integral modeling was primarily regarded as a numerical tool for solving incompressible, irrotational, steady inviscid potential flows. A succession of research workers have extended the surface vorticity model proposed originally by E. Martensen[1] to deal with a wide range of practical engineering situations. These include the flow past airfoils, slotted airfoils, cascades, axial, radial, and mixed-flow turbomachine cascades, axisymmetric annuli, bodies of revolution, ducts, and ducted propellers or fans. Much of this work has been reviewed by the present author.[2]

The present article is aimed at the extension of the surface vorticity method to deal with flows that involve free shear layers or jets. Four classes of such flows may be identified, as follows:

(1) free streamline modeling of separated flow;
(2) deflection of jets by an oblique surface;
(3) flow past a lifting body situated in a jet with consequent jet reaction;
(4) models for the inverse design of airfoils or cascades.[3]

A boundary integral formulation to handle the first three of these problems is presented in this article. Following an initial development of relevant fluid dynamic models and basic equations in Section 2.0, solutions for free streamline flows are given in Section 3.0. These are the stepping stones to consideration of the more important applications of jet flows developed in Section 4.0.

Item (4) has been dealt with fully by the author elsewhere[3] in relation to the design of airfoils and cascades for a prescribed surface pressure distribution. The body is modeled by a flexible vortex sheet of prescribed strength, which is readjusted iteratively to coincide with its self-induced streamline. Similar techniques are used herein to determine the self-convecting influence of the free vortex sheets used to simulate the free streamlines and jets.

There is a considerable literature on bluff body wake flows employing other modeling techniques, typical of which are reports by G. V. Parkinson and T. Jandali[4] and P. W. Bearman and J. E. Fackrell,[5] stemming from earlier work by A. Roshko.[6] The latter used a hodograph method combined with conformal transformation from the circle plane to model free streamline flows. Parkinson and Jandali[4] improved on this to avoid complex procedures of the hodograph method. Unlike the present work, which seeks to model the motionless wake of a true free streamline flow, these authors introduced sources on the rear body surface to exercise control over the pressure at the separation point, which was then assumed to equal the base pressure. Bearman and Fackrell[5] generalized the numerical model by the introduction of discrete vortex modeling of the wetted body surface, also introducing source strength on two surface elements of the wake to gain control over wake pressure as a means for correlating with experiment. All these authors sought to model the averaged bluff body flows with attention focused on the near body flow and drag coefficient. No attempt was made to include the induced effects of the separated vortex sheets that extend to infinity downstream, as in the present work, since these were in effect replaced by the wake sources introduced to simulate base pressure of real flows.

Address reprint requests to Professor Lewis at the Department of Mechanical, Materials and Manufacturing Engineering, University of Newcastle upon Tyne NE1 7RU, UK.

Received 24 April 1990; accepted 11 September 1990

2.0 Vortex sheet model for potential flows and free shear layer flows

Among computational techniques, surface vorticity boundary integral methods offer the distinct advantage of attempting to simulate directly the principal driving mechanism of fluid motions, namely vorticity generation at a body surface. In all real flows, surface vorticity thus created is diffused into the boundary layer where it is convected downstream and is ultimately shed into the wake. Free streamline modeling provides a simple technique for handling this vortex-shedding process for irrotational inviscid flows. Figures 1b and c illustrate the use of vortex sheets to simulate these two types of potential flow by boundary integral analysis. In both cases the flow regime is divided between two domains separated by a free vortex sheet, which is aligned with and convected by the local velocity. The outer domain covers the whole active flow field, while the inner domain contains a core of motionless fluid, representing either the region blocked out by a body or the wake extending to infinity downstream.

2.1 Free vortex sheet

Some useful relationships may be derived if we consider first

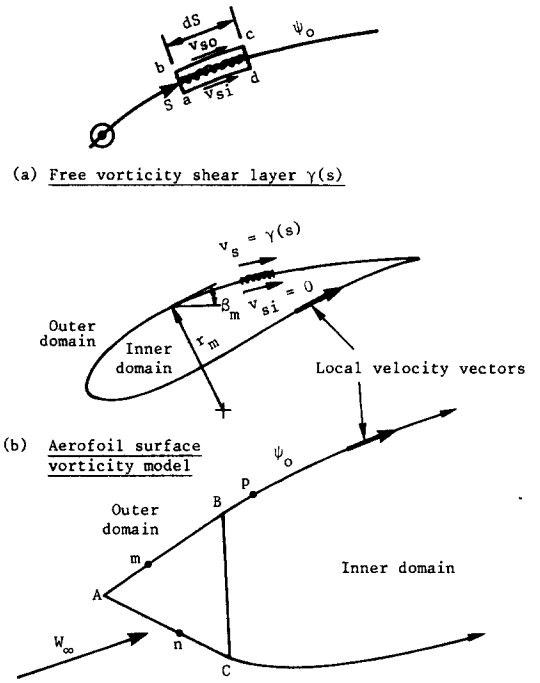

Figure 1 Free shear layer models

the more general situation depicted by Figure 1a involving a freely convecting vortex sheet of strength $\gamma(s)$ per unit length, which divides two flow regimes of different stagnation pressures p_{oo} and p_{oi}. Since the sheet is aligned with the bounding streamline ψ_o, the vortex strength may be related directly to the velocity jump across the sheet from v_{si} to v_{so}. By taking the circulation about the element ds following contour $abcd$ and with clockwise positive notation, we then have the relationship

$$\gamma(s) = v_{so} - v_{si} \tag{1}$$

The convection velocity of the sheet can also be expressed through

$$v_{sc} = \tfrac{1}{2}(v_{so} + v_{si}) \tag{2}$$

For a freely convecting vortex sheet, the static pressure is constant across the sheet. Consequently, the stagnation pressure jump across the sheet may be derived through

$$\frac{1}{\rho}(p_{oo} - p_{oi}) = \tfrac{1}{2}(v_{so}^2 - v_{si}^2) = v_{sc}\gamma(s) \tag{3}$$

Since stagnation pressure is conserved in the two inviscid irrotational domains, it follows that $v_{sc}\gamma(s)$ remains constant along the vortex sheet once shed into the fluid. In the case of the free streamline flow, Figure 1c, since $v_{si} = 0$, Equations 1–3 reduce to

$$\begin{aligned} &\gamma(s) = v_{so} = W_\infty \\ &v_{sc} = \tfrac{1}{2}W_\infty \\ &\frac{1}{\rho}(p_{oo} - p_{oi}) = \tfrac{1}{2}W_\infty^2 \end{aligned} \tag{4}$$

A free streamline may thus be modeled by enforcing a constant vortex sheet strength of $\gamma(s) = W_\infty$ (i.e., the value of the superimposed uniform stream). The convection velocity of the sheet is then constant ($v_{sc} = \frac{1}{2}W_\infty$), and likewise the velocity at the outer domain surface of the sheet is constant and equal to W_∞. These simple rules are applied in the free stream and jet analyses presented in Sections (4.0) and (5.0).

2.2 Vortex sheets "bound" to a body surface

As illustrated by Figure 1b, the slip flow at a body surface in potential flow may also be treated as a vortex sheet, but in this case bound to the surface. Following Martensen[1] and Lewis,[2] the boundary condition at the body surface of parallel flow can be enforced if the velocity v_{si} just inside the vortex sheet and parallel to the surface is set equal to zero. Equations 1 and 2, then, reduce to

$$\begin{aligned} &\gamma(s) = v_s \\ &v_{sc} = \tfrac{1}{2}\gamma(s) \end{aligned} \tag{5}$$

where v_s is the local surface potential flow velocity.

The vortex sheet is thus bound only in the sense that it remains in contact with the body surface in potential flows. In fact the vortex sheet is convected with velocity v_{sc} equal to one half the local surface vortex strength in the downstream direction parallel to the surface. Furthermore, unlike the free

Notation

a_{mn}	Distance between m and n
b_{mn}	Distance between m and reflection of n in x axis
C_L	Lift coefficient
h	Jet width
H	Wind tunnel open jet width
$K(s_m, s_n)$	Coupling coefficients
$\bar{K}(s_m, s_n)$	Coupling coefficients
$L(s_m, s_n)$	Coupling coefficients
$\bar{L}(s_m, s_n)$	Coupling coefficients
l	Airfoil chord
m, n, p, q	Locations on vortex sheets
p	Static pressure
p_o	Stagnation pressure
r_m	Radius of curvature of body surface at m
s	Distance along body surface
t	Time
u, U	Velocity components in x direction
v, V	Velocity components in y direction
v	Surface velocity
W_∞	Absolute velocity, $\hat{i}U_\infty + \hat{j}V_\infty$
x, y	Cartesian coordinates

Greek symbols

α_∞	Angle of attack
β	Slope of blade surface relative to x axis
ϕ_∞	Vector mean angle
$\gamma(s)$	Surface vorticity strength
$\Gamma(s)$	Free vorticity sheet strength

Subscripts

c	Convection velocity
i	Inner domain
o	Outer domain
m, n, p, q	Points on a vortex sheet
s	On a body surface or vortex sheet
∞	At infinity

streamline vortex sheets that we just considered, Equation 4, its strength $\gamma(s)$ is not constant but varies along the body surface, being equal to the local potential flow velocity v_s, as shown by Equation 5. Surface vorticity is thus created or destroyed continuously as the sheet convects along the body surface. By application of the circulation theorem to the elementary control volume *abcd* (see Figure 1a), we may then show[2,7] that vorticity production is related to local surface pressure gradient through

$$\frac{d\gamma}{dt}=\frac{d}{ds}\left(\frac{v_s^2}{2}\right)=-\frac{1}{\rho}\frac{dp}{ds} \tag{6}$$

Since the interior domain can be regarded for flow-modeling purposes as filled with motionless (stagnant) fluid, the internal static pressure must be constant and equal to the stagnation pressure of the outer domain. Equation 3 derived for free shear layers is thus no longer applicable, since there is now a pressure jump across the vortex sheet associated with its being bound to the surface. The binding force dF on a sheet element ds follows from the Magnus law, namely,

$$\begin{aligned} dF&=\rho v_{sc}\gamma(s)\,ds \\ &=(p_i-p) \end{aligned} \tag{7}$$

Introducing Equation 5, we have finally

$$p_i=p+\tfrac{1}{2}\rho v_s^2=p_o \tag{8}$$

confirming that the static pressure of the inner domain p_i is indeed equal to the stagnation pressure p_o of the outer domain.

Moving on now to practical computations, the body boundary condition $v_{si}=0$ for any point m (see Figure 1c), may be stated as a boundary integral equation of the following form for a flow regime involving also Q free streamlines:

$$\begin{aligned} &-\tfrac{1}{2}\gamma(s_m)+\oint K(s_m, s_n)\gamma(s_n)\,ds_n+\hat{W}_\infty\cdot\hat{d}s_m \\ &+\sum_{q=1}^{Q}\Gamma_q\int K(s_m, s_p)\,ds_p=0 \end{aligned} \tag{9}$$

where running points n and p are located on the body surface and the free streamline, respectively. The free vortex sheet strength is denoted by Γ_q. Equation 9 includes contributions to v_{si} at any body point m due to all influences present in the flow regime, namely,

(1) the velocity discontinuity $-\frac{1}{2}\gamma(s_m)$ at s_m;
(2) the bound vorticity $\gamma(s_n)$;
(3) the uniform stream W_∞;
(4) the free streamline vorticity Γ_q.

The Kernel functions $K(s_m, s_n)$ and $K(s_m, s_p)$ are called coupling coefficients, linking points n and p to the body boundary point m.

2.3 Numerical representation

If the integrals are evaluated by the trapezium rule, Equation 9 may be written more simply as

$$\sum_{n=1}^{N}\bar{K}(s_m, s_n)\gamma(s_n)=-(U_\infty+U_m)\cos\beta_m-(V_\infty+V_m)\sin\beta_m \tag{10}$$

where (U_∞, V_∞) are the (x, y) components of the superimposed uniform stream W_∞ and where (U_m, V_m) are the velocity components induced at m by the Q free vortex sheets, namely,

$$\begin{aligned} U_m&=\frac{1}{2\pi}\sum_{q=1}^{Q}\left\{\Gamma_q\sum_{p=1}^{P}\left[\frac{y_m-y_p}{a_{mp}^2}\right]\Delta s_p\right\} \\ V_m&=\frac{1}{2\pi}\sum_{q=1}^{Q}\left\{\Gamma_q\sum_{p=1}^{P}\left[\frac{x_p-x_m}{a_{mp}^2}\right]\Delta s_p\right\} \end{aligned} \tag{11}$$

where

$$a_{mp}=\sqrt{(x_p-x_m)^2+(y_p-y_m)^2} \tag{12}$$

The modified coupling coefficients $\bar{K}(s_m, s_n)$ are given by

$$\begin{aligned} \bar{K}(s_m, s_n)&=\frac{\Delta s_m}{2\pi}\left\{\frac{(y_m-y_n)\cos\beta_m-(x_m-x_n)\sin\beta_m}{a_{mn}^2}\right\} && \text{for } n\neq m \\ &=-\frac{1}{2}+\frac{\Delta s_m}{4\pi r_m} && \text{for } n=m \end{aligned} \tag{13}$$

where β_m is the body profile slope, r_m its local radius of curvature (see Figure 1b), and

$$a_{mn}=\sqrt{(x_m-x_n)^2+(y_m-y_n)^2} \tag{14}$$

Reduction of the boundary integral Equation 9 to its quadrature equivalent Equation 10 implies the introduction of finite numbers N and P of discrete sheet vortex elements Δs_n and Δs_p to represent the body surface and free streamlines, respectively. In the absence of free streamlines, Equation 10 reduces still further to

$$\sum_{n=1}^{N}\bar{K}(s_m, s_n)\Delta(s)_n=-U_\infty\cos\beta_m-V_\infty\sin\beta_m \tag{15}$$

the governing equation for plane two-dimensional (2-D) potential flows. The problem then reduces to the solution of N such equations, one for each element, yielding the N initially unknown values of surface vorticity $\gamma(s_n)$ and hence, via the first Equation 5, the surface velocity v_s.

For free streamline problems, on the other hand, the additional terms U_m and V_m on the right-hand side of Equation 10 are not initially determinate. Although the vortex sheet strength has a prescribed value $\Gamma_p=W_\infty$, as shown in Section 2.1, its shape (x_p, y_p) is not known initially and must be found by iterative techniques involving successive approximations that are described later. At each iteration, however, with current estimates of (x_p, y_p), the right-hand side of Equation 10 becomes fully determined making use of Equations 11, so that solutions for $\gamma(s_n)$ may be obtained.

3.0 Free streamline analysis

A model and strategy for simulation of a free streamline flow are shown in Figure 2, which depicts the flow past a wedge-shaped obstacle located in a uniform stream U_∞. The free streamline ψ_o, which separates from the sharp corner P, is coincident with a vortex sheet PR extending to $x=\infty$ and of strength $\Gamma(s)=U_\infty$. It follows from the discussion in Section 2.1 that the fluid within the wake region BPR is then motionless. The proposed flow model thus encompasses the following:

(i) a vortex sheet of initially unknown strength $\gamma(s)$ bound to the prescribed body surface APB, represented by M discrete elements;
(ii) a shed vortex sheet PRQ of prescribed strength $\Gamma(s)=U_\infty$ made up of a flexible curved section PR containing P vortex elements and a straight section RQ extending to $x=\infty$ to complete the wake closure;
(iii) a mirror image of (i) and (ii) below the x axis to enforce symmetry about the x axis;
(iv) a uniform stream U_∞ parallel to the x axis;
(v) a boundary condition of zero velocity on and parallel to the inner surface APB of the body;
(vi) a similar boundary condition on the inner surface of the free vortex sheet PR.

This last condition is met automatically provided the vortex sheet lies along the separated free streamline. Clearly, wake closure presents a dilemma here since computational practicality limits the allowable number of wake elements P. The use of a semi-infinite vortex sheet RQ as proposed in (ii) is thus a necessary but not altogether satisfactory compromise and one that can lead to errors, as we will show.

An appropriate computational sequence may be summarized as follows:

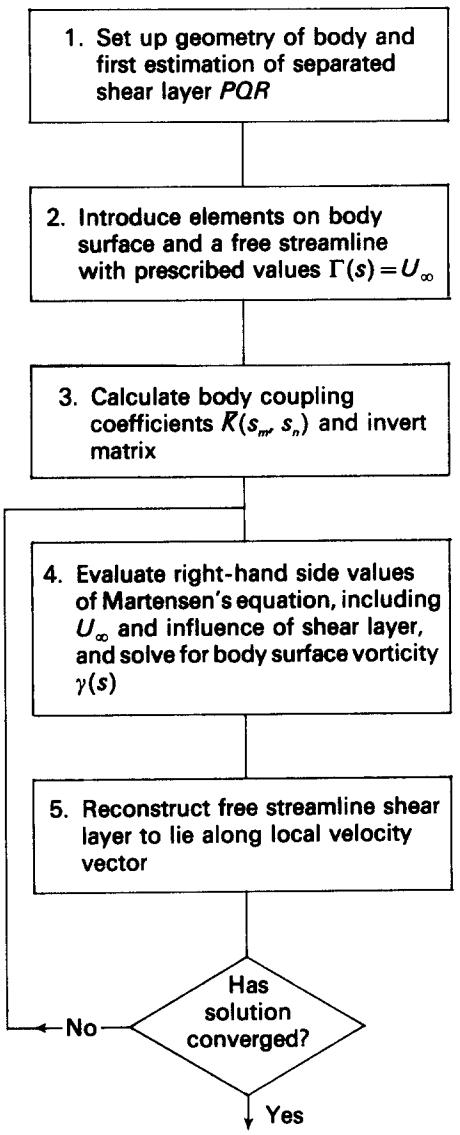

To complete the specification of this flow model, the equations referred to in the flow diagram are as follows. Martensen's Equation 10 may be modified to include the semi-infinite vortex sheets by the introduction of additional induced velocities (U_{om}, V_{om}). We then have

$$\sum_{n=1}^{N} L(s_m, s_n)\gamma(s_n) = -(U_\infty + U_m + U_{om}) \times \cos\beta_m - (V_\infty + V_m + V_{om}) \sin\beta_m \tag{16}$$

where

$$U_{om} = \frac{U_\infty}{2\pi}(\phi_{2m} - \phi_{1m})$$
$$V_{om} = \frac{U_\infty}{2\pi} \ln\left(\frac{b_{om}}{a_{om}}\right) \tag{17}$$

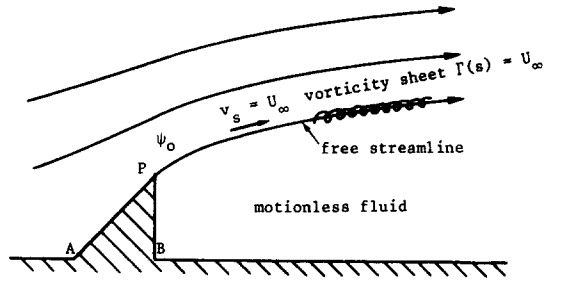

(a) Free streamline separation from a ridge

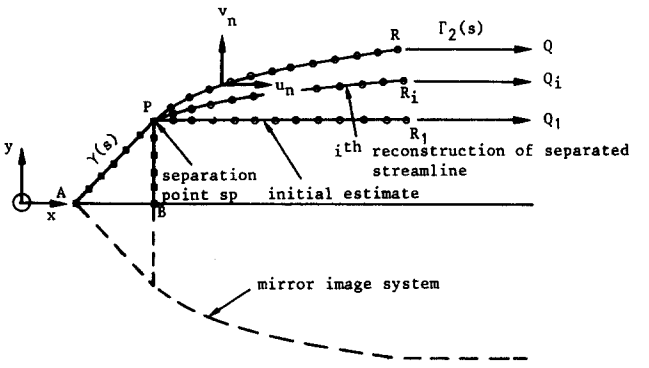

(b) Surface vorticity mirror image model

Figure 2 Surface and free vorticity model of "free streamline" flow separation from a sharp-edged ridge

with

$$\phi_{1m} = \pi - \arctan\left(\frac{y_m - y_r}{x_r - x_m}\right)$$
$$\phi_{2m} = \pi - \arctan\left(\frac{y_m + y_r}{x_r - x_m}\right) \tag{18}$$
$$a_{om} = \sqrt{(y_m - y_r)^2 + (x_m - x_r)^2}$$
$$b_{om} = \sqrt{(y_m + y_r)^2 + (x_m - x_r)^2}$$

The velocities induced at m on the body due to the flexible free vortex sheet PR of strength $\Gamma(s_p) = U_\infty$ and its mirror image, are given by

$$U_m = \sum_{p=1}^{P} \Gamma(s_p)\,\Delta s_p\,\bar{u}_{mp}$$
$$V_m = \sum_{p=1}^{P} \Gamma(s_p)\,\Delta s_p\,\bar{v}_{mp} \tag{19}$$

where $\bar{u}_{mp}$ and $\bar{v}_{mp}$ are the velocity components at m induced by a point vortex pair at $x = x_p$ and $y = \pm y_p$, namely,

$$\bar{u}_{mp} = \frac{1}{2\pi}\left(\frac{y_m - y_p}{a_{mp}^2} - \frac{y_m + y_p}{b_{mp}^2}\right)$$
$$\bar{v}_{mp} = \frac{1}{2\pi}\left(\frac{1}{a_{mp}^2} - \frac{1}{b_{mp}^2}\right)(x_o - x_m) \tag{20}$$

with

$$a_{mp} = \sqrt{(x_m - x_p)^2 + (y_m - y_p)^2}$$
$$b_{mp} = \sqrt{(x_m - x_p)^2 + (y_m + y_p)^2} \tag{21}$$

Use of the unit vortex pair velocities given by Equations 20 may be made to evaluate the modified coupling coefficients $L(s_m, s_n)$ in the governing Equation 16, which becomes

$$L(s_m, s_n) = \bar{u}_{mn}\,\Delta s_n \cos\beta_m + \bar{v}_{mn}\,\Delta s_n \sin\beta_m \qquad \text{for } m \neq n \qquad (22)$$

For the special case $m = n$, which accounts for the self-induced effects of element m, element curvature must be included, following Equations 13, but including also the velocity in the x direction induced by the mirror image vortex element. We then have

$$L(s_m, s_m) = -\frac{1}{2} + \frac{\Delta s_m}{4\pi r_m} - \frac{\Delta s_m}{4\pi y_m}\cos\beta_m \qquad (23)$$

Use may also be made of the unit vortex pair velocities, Equations 20, for the computations required in step 4 of the preceding flow diagram to reconstruct the free streamline at the conclusion of each iteration. The velocity components at the center of element m on the free streamline are then given by

$$u_m = U_\infty + \sum_{n=1}^{N} \gamma(s_n)\,\Delta s_n\,\bar{u}_{mn} + \sum_{p=1}^{P} U_\infty\,\Delta s_p\,\bar{u}_{mp} + \frac{\Delta s_m}{4\pi r_m}\cos\beta_m - \frac{\Delta s_m}{4\pi y_m} + U_{om} \qquad (24)$$

$$v_m = \sum_{n=1}^{N} \gamma(s_n)\,\Delta s_n\,\bar{v}_{mn} + \sum_{p=1}^{P} U_\infty\,\Delta s_p\,\bar{v}_{mp} + \frac{\Delta s_m}{4\pi r_m}\sin\beta_m + V_{om}$$

After convergence, the velocity v_s' on the outer surface of the free vortex sheet resulting from the numerical model may be derived from Equations 2 and 4 (first), namely,

$$v_s' = 2\sqrt{u_m^2 + v_m^2} \qquad (25)$$

This value can be compared with the prescribed value U_∞ as a further check on the accuracy of the numerical simulation.

3.1 Application to wedge and plate separating flows

The application of this method to free streamline flow separation from a wedge-shaped body is shown in Figure 3, for which the flexible vortex sheet PR was limited in length to about $6 \times AP$. Convergence was obtained with 30 iterations. Two studies are compared in Figure 3. With the sheet vortex strength set at its correct value $\Gamma(s) = U_\infty$, the numerical method seriously underestimated the free streamline deflection (curve 2). The reason for this is almost certainly the problem of leakage flux due to failure to satisfy any boundary conditions on the semi-infinite vortex wake RQ. Evidence for this was the presence of significant velocity on the rear-facing surface PB of the body, signifying noticeable fluid motion within the wake region. To compensate for this, the free streamline sheet strength $\Gamma(s)$ was increased progressively, providing additional backwash, until a value was found for which the surface velocity on the rear face PB was negligible ($v_s/U_\infty < 0.01$). As can be seen from curve 3, the value $\Gamma(s)/U_\infty = 1.15$ then produced an extremely good prediction of the free streamline contour.

Flow past a sharp-edged plate normal to U_∞, Figure 4, presents testing conditions in which the vortex sheet separates at right angles to the uniform stream. After similar experimentation, extremely good predictions were obtained. In this case we found it advantageous to adopt different values of $\Gamma_1(s)$ for the flexible vortex sheet and $\Gamma_2(s)$ for the downstream semi-infinite vortex sheet. After some experimentation, values of $\Gamma_1(s) = 1.19$ and $\Gamma_2(s) = 1.29$ produced optimum results. Good predictions were obtained for the velocity on the plate surface in comparison with exact free streamline analysis, Figure 5, and also the free streamline contour, Figure 4.

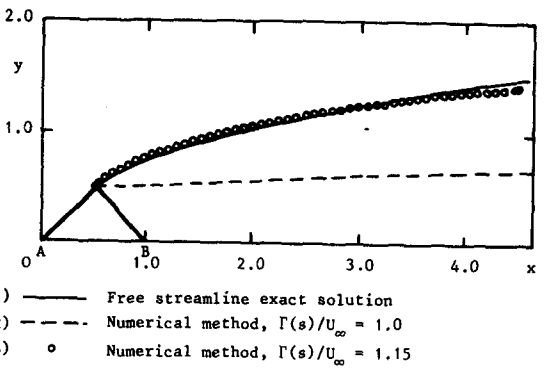

Figure 3 Free streamline flow from a wedge-shaped body

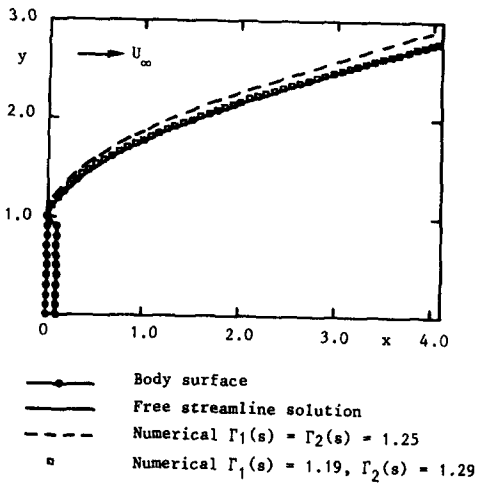

Figure 4 Free streamline separation from a sharp-edged plate

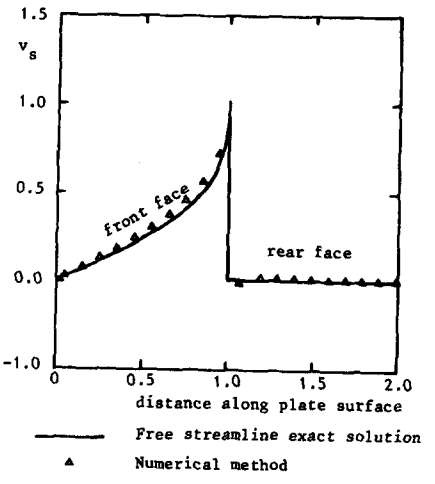

Figure 5 Velocity distribution along surface of sharp-edged plate in free streamline separated flow

4.0 Free jets

This numerical model readily may be extended to deal with jet flows by the introduction of additional vortex sheets. Figure 6 illustrates an appropriate strategy for setting up a vortex sheet structure suitable for simulating the deflection of a jet stream of thickness h by a wedge-shaped obstacle APB, involving the

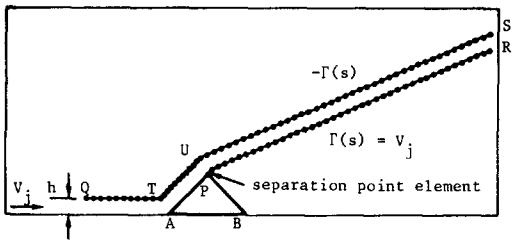

Figure 6 Initial specification of vortex sheet model for flow of a jet over a ridge

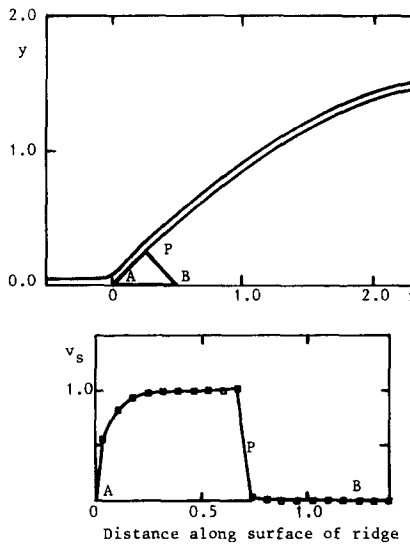

Figure 7 Prediction of jet deflection and associated body surface velocity distribution

introduction of a second flexible vortex sheet $QTUS$ to form the upper surface of the jet. Entry flow may be achieved by the introduction of a semi-infinite vortex sheet extending from $-\infty$ to point Q and of strength $\Gamma(s)$ equal to the jet velocity V_j. In this problem the superposition of a uniform stream is not required, since the vortex sheets themselves are able to introduce the jet entry and exit fluxes.

However, such an arrangement requires prior knowledge of the jet angle for correct orientation of the downstream semi-infinite vortex sheet pair. This angle can be estimated during the iterative procedure from the predicted pressure distribution experienced by the deflector and upstream wall. However, a simpler approach, which leads to acceptable solutions, is to omit the downstream semi-infinite vortex sheet pair completely, allowing the exit flux to vent freely. A solution on this basis with $h=0.1$ for a wedge height of 1.0 and a jet velocity $V_j=\Gamma(s)=1.0$, is shown in Figure 7. The iterative procedure follows that of the flow diagram for free streamline flow in Section 3.0, involving successive reconstruction of the jet shape from some initial first guess such as that shown in Figure 6. Although the jet exit flow causes erroneous curvature of the jet in its exit region, the effect of this on the near field can be minimized by extending the jet far enough downstream. The solution is then acceptable close to the ridge and the surface velocity distribution is likewise acceptable. The velocity builds up to approximately 1.0 on the upwind face AP beginning with stagnation conditions at A, and velocities are negligible on the rear face PB, as expected.

Another device that helps minimize exit jet curvature is to introduce a sink into the jet stream at its downstream end of precisely the correct strength $S=-V_j h$ to absorb all the jet mass flow. This helps to compensate for backwash due to leakage flux, which otherwise occurs with the freely venting model.

A significant improvement is also obtained by the introduction of some constraint over the direction of flow separation of the lower vortex sheet at P. Best results are obtained if the first element leaving the separation point is set to the body profile slope upstream of the separation point, as indicated in Figure 6, and maintained at this angle throughout the computation. Such arrangements considerably improve predictions for both jet and free streamline flows.

4.1 Simulation of an open jet wind tunnel test section

The sheet vorticity boundary integral method presented in this article may be easily adapted to a wide range of problems, and we conclude with a brief outline of its application to the modeling of an open jet wind tunnel. Further details have been given in Reference 8. The scheme is illustrated in Figure 8, which depicts an airfoil of chord l located in the open jet just downstream of a wind tunnel nozzle of width H. To maintain 2-D flow, top and bottom walls are provided to contain the jet, which is otherwise free to deflect in reaction to the force developed by the airfoil. The theoretical simulation assumes 2-D flow.

The main attractions of this method for obtaining experimental lift/drag data are (a) its cheapness and simplicity and (b) minimization of wind tunnel interference as a result of the imposition of constant atmospheric pressure on each side of the jet. The main disadvantage is the problem of jet deflection, which causes the local angle of attack α_∞ perceived by the airfoil to differ from its blade setting angle β (Figure 8). There is no certain way of evaluating the angle of attack α_∞ experimentally, the normal practice being to measure the jet efflux angle θ and to assume that W_∞ is the vector mean of the upstream and downstream jet velocities W_1 and W_2. The vector mean flow angle in the test section is then given by

$$\phi_\infty = \frac{\theta}{2} \tag{26}$$

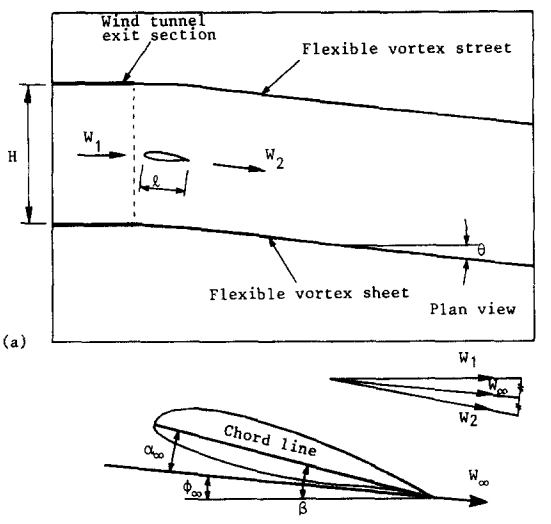

Figure 8 Flow model for simulation program "Aerojet"

and the angle of attack becomes

$$\alpha_\infty \approx \beta - \frac{\theta}{2} \tag{27}$$

As shown in Reference 8, however, and illustrated by Figure 9, this leads to significant errors, which are beyond experimental investigation and can only be evaluated through a full theoretical simulation. The foregoing boundary integral method has proved a powerful, accurate, and revealing research tool in this respect. The simulation involved the introduction of two flexible free vortex sheets to model the open jet, extending downstream to a distance of $10H$. The jet flow was initiated by two

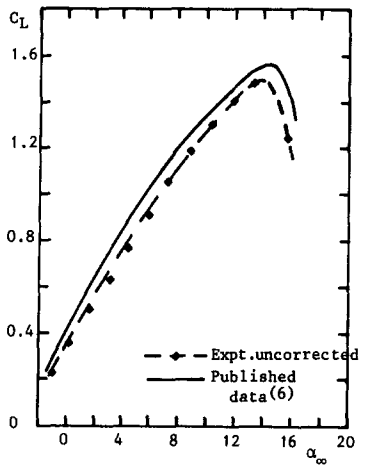

Figure 9 Comparison of published $C_L - \alpha_\infty$ data[9] with uncorrected data from open jet wind tunnel tests[6]

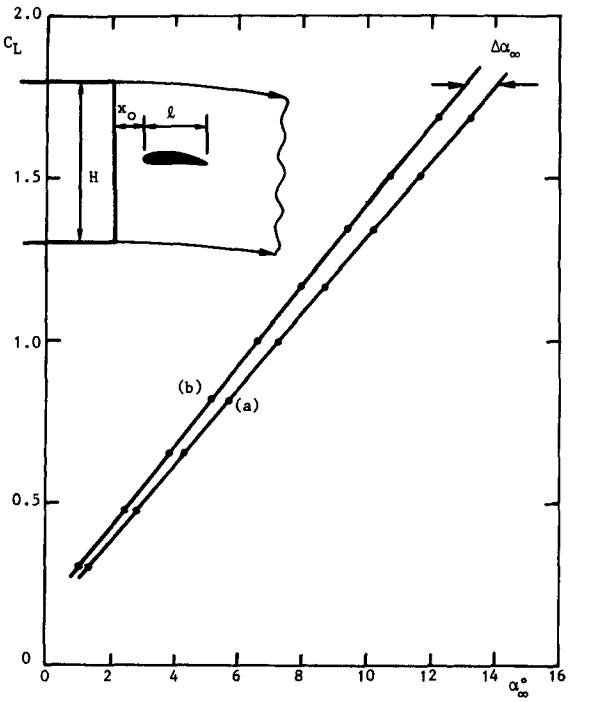

Figure 10 Theoretical predictions of frictionless $C_L - \alpha_\infty$ characteristics for NASA LS(1)-0417 MOD

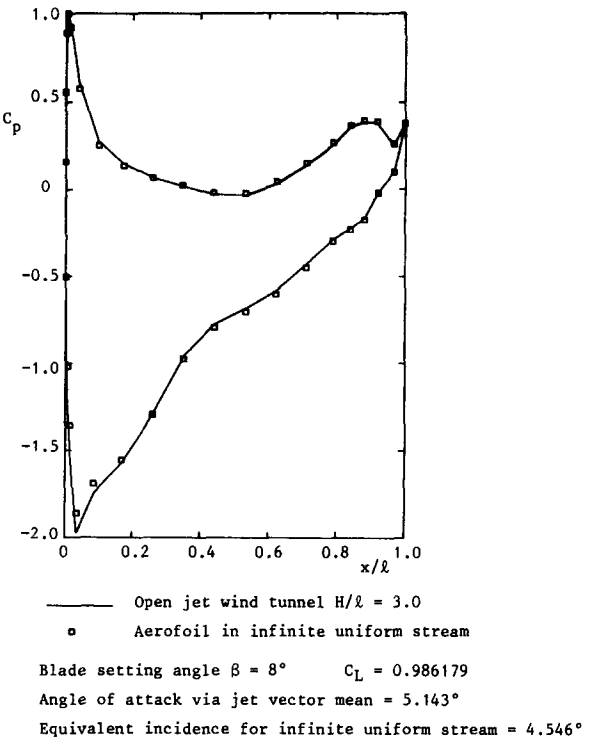

Figure 11 Predicted surface pressure distribution for NASA LS(1)-0417 MOD in open jet wind tunnel and infinite uniform stream for same lift coefficient

semi-infinite vortex sheets distance H apart and extending between $-\infty < x < 0$ to simulate the wind tunnel nozzle exit section. Downstream the jet efflux was terminated by a sink of strength HW_∞ placed midway between the last two elements of the flexible vortex jet bounding sheets. The airfoil itself was modeled by a surface vorticity distribution $\gamma(s)$ employing the "Wilkinson" statement of the Kutta Joukowski trailing edge condition.[2]

A second airfoil surface vorticity computer simulation was also undertaken, involving (instead of the jet) an infinite uniform stream $W_\infty = \hat{i}U_\infty + \hat{j}V_\infty$. This program was so arranged that unit solutions were first obtained by $U_\infty = 1.0$ and $V_\infty = 1.0$. For any prescribed lift coefficient, it is then a relatively easy matter to find the angle of attack α_∞ that will recombine the unit solutions scaled by $U_\infty = W_\infty \cos\alpha_\infty$ and $V_\infty \sin\alpha_\infty$ to yield the prescribed lift coefficient. Applying this technique to airfoil NASA LS(1)-0417 MOD, two $C_L - \alpha_\infty$ curves were obtained (Figure 10), one for the jet flow model, curve (a), and the second for the true airfoil flow with identical lift coefficient, curve (b). The outcome of this study was the evaluation of an angle of attack correction $\Delta\alpha_\infty$. Application of this to the experimental data of Figure 9 results in extremely good agreement between the experimental results and published data.[9]

As a more detailed check on the viability of the jet simulation, the predicted surface pressure distribution is compared in Figure 11 with that of the true uniform stream flow for an identical lift coefficient $C_L = 0.986179$. This confirms that the detailed flow distribution on the airfoil surface was accurately simulated for a jet width/chord ratio of $H/l = 3.0$, the correction angle being $\Delta\alpha_\infty = 0.597°$. Using this technique, we should modify Equation 27 to read

$$\alpha_\infty = \beta - \frac{\theta}{2} - \Delta\alpha_\infty \tag{27a}$$

Acknowledgments

The author wishes to thank Roberta Stocks for her help in producing the manuscript and I. Potts and A. A. Arain for the experimental test result quoted in Figure 9.

References

1 Martensen, E. Berechnung der Druckverteilung an Gitterprofilen in ebener Potentialstromung mit einer Fredholmschen Integralgleichung. *Arch. Rat. Mech. Anal.*, 1959, **3**, 235–270

2 Lewis, R. I. *Vortex Element Methods for Fluid Dynamic Analysis of Engineering Systems*. To be published by Cambridge University Press, January, 1991

3 Lewis, R. I. A method for inverse aerofoil and cascade design by surface vorticity. ASME Paper No. 82-GT-154, 1982

4 Parkinson, G. V. and Jandali, T. A wake source model for bluff body potential flow. *J. Fluid Mech.*, 1970, **40**(3), 577–594

5 Bearman, P. W. and Fackrell, J. E. Calculation of two-dimensional and axisymmetric bluff body potential flow. *J. Fluid Mech.*, 1972, **72**(2), 229–241

6 Roshko, A. A new hodograph for free streamline theory. NACA TN 3/68, 1954

7 Lewis, R. I. Surface vorticity modelling of separated flows from two-dimensional bluff bodies of arbitrary shape. *J. Mech. Eng. Sci.*, 1981, **23**(1), 1–12

8 Lewis, R. I., Potts, I., and Arain, A. A. Preliminary studies of leading edge spoilers for lift/drag control of wind turbine generators. Final Report on E.T.S.U. Agreement No. E/5A/CON/5125/2010, April 1990

9 Miley, S. J. A catalogue of low Reynolds number airfoil data for wind turbine applications. Dept. of Aerospace Engineering, Texas A. & M. University (part of U.S.D. of E. Wind Energy Tech. Div., Fed. Wind Energy Prog., Contract No. DE-AC-04-76DP03533), 1982